A Letters Journal Exploring the Frontiers of Physics

October 2013

EPL, **104** (2013) 14005
doi: 10.1209/0295-5075/104/14005

www.epljournal.org

Spooling and disordered packing of elastic rods in cylindrical cavities

M. Piñeirua[1,2], M. Adda-Bedia[1] and S. Moulinet[1]

[1] *Laboratoire de Physique Statistique, Ecole Normale Supérieure, UPMC Paris 6, Université Paris Diderot, CNRS 24 rue Lhomond, 75005 Paris, France*
[2] *ENSTA ParisTech, Unité de Mécanique - Chemin de l'Hunière, 91761 Palaiseau, France*

received 2 August 2013; accepted in final form 10 October 2013
published online 1 November 2013

PACS 46.32.+x – Static buckling and instability
PACS 46.70.Hg – Membranes, rods, and strings
PACS 61.43.-j – Disordered solids

Abstract – The compaction of elastic rods in rigid cylindrical cavities is experimentally performed. The results show two main packing behaviours: an ordered regime in which the rod spools on the internal surface of the cavity and a disordered phase where the orientation of the coils is randomly distributed. The phase diagram separating these two packing configurations is determined as a function of the aspect ratio of the container and of the intrinsic curvature of the rod. A theoretical stability analysis and an experimental study of the dynamics of the rod at the injection point allow to describe different instability mechanisms that drive the transitions from ordered to disordered packing, leading to the identification of the different disordering scenarios.

Many natural phenomena and man-made systems feature confined elastic structures, such as plates and rods, which are mechanically and geometrically constrained by some outer embedding receptacle [1–7]. In order to fit into a smaller space than their normal linear extension, these elastic structures are forced to undergo large deformations whereupon geometrical self-avoidance looms in the form of intricate non-local interactions. These folding, wrinkling and crumpling processes range from the nano- to the macro-scale and the confinement itself can either serve a biological purpose, such as the protective bud enclosing growing tree leaves [1,2], or an engineering objective, such as self-deployable solar sails [3] or drill strings in oil ducts [4]. In this case, the post-buckling behaviour of a twisted elastic rod under axial compression or tension while being simultaneously tightly secured inside a cylindrical cavity is of particular importance for the oil extraction industry [4]. In microbiology, physical models based on the elasticity of rods are used to determine the mechanical forces that are involved in the packing of DNA filaments, the evolution of their complex folding configurations and their subsequent ejection in and out of virus capsids, *i.e.* processes essential to the life cycles of viruses [5–7].

Confined macroscopic elastic structures have come forth as a novel class of frustrated and disordered systems elevating them, alongside granular materials, as a model of complex athermal systems. In fact, it has been shown that many aspects of glassy systems such as logarithmic ageing [8,9] and the pertinence of statistical distributions are well-suited tools to investigate the complex energy landscape experienced by tightly packed elastic plates and rods [10–14]. Besides their elastic properties, the crucial ingredients responsible for the analogy between athermal glassy systems and tightly packed elastic rods and plates are geomerical self-avoidance and energy dissipation via friction. One important difference with molecular glasses stems from the fact that thermal fluctuations play no role in the phase-space exploration of a macroscopic folded elastic rod thereby raising challenging questions such as potential ergodicity breaking.

An important stepping stone still standing in the way concerns the necessity of achieving a more precise understanding of the possible compaction morphologies. Previous studies of confined elastic rods inevitably required elaborate experimental techniques in order to visualize and measure the geometrical properties of the folded rods [15–17]. This is because the interior of the confining cavity cannot easily be accessed by traditional image analysis tools [17]. Here, we propose a new approach based on the analysis of the rod dynamics at both the injection point and inside the cavity that allows to describe

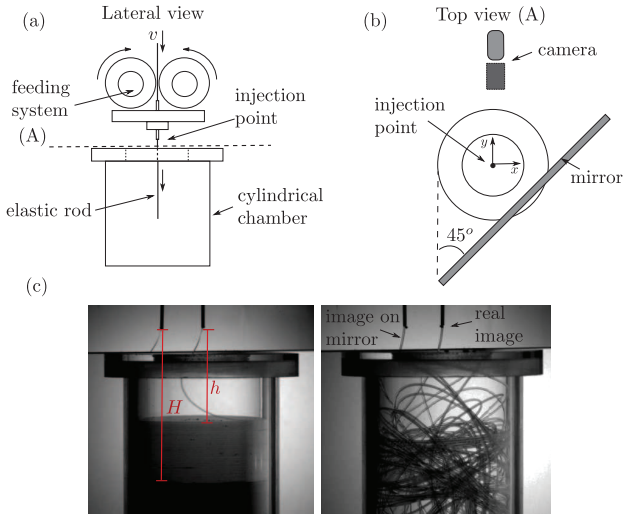

Fig. 1: (Colour on-line) Lateral (a) and top (b) views of the experimental setup for the injection of a flexible rod inside a cylindrical cavity. (c) Two examples of confined configurations showing both spooling (left) and disordered packing (right).

accurately the geometrical and dynamical properties of the packing process. This letter addresses the origin of the emerging ordered and disordered packing configurations, and culminates with a prediction about the transition between these two phases depending on the geometrical parameters of the experimental system.

The experimental setup consists of a cylindrical plexiglass chamber with a circular hole in the top cover to allow the entrance of the elastic rod. The role of the top cover is to prevent the rod from possibly leaving the cylindrical chamber during compaction. Two rollers turning at constant speed push the rod through an injector into the cylindrical chamber (fig. 1(a)). The feeding speed v has been checked to be small enough for the compaction process to be quasistatic. The tip of the injector is placed along the centre of the container at 10 mm above the top cover. A CCD camera registers the lateral view of the system during packing at a rate of 10 images per second. A mirror is placed behind the injection point at 45° with respect to the optical axis of the camera (fig. 1(b)) in order to recover the local position of the rod in the plane lying parallel to the cylinder's top cover. The diameter of the entrance hole insures that the rod does not touch the cover, so that the injection dynamics is not affected. In the captured images (fig. 1(c)), the real and reflected images on the mirror determine directly the x and y positions of the rod, respectively (the distance from the camera to the rod is much larger than the distance between the mirror and the rod).

Circular rods of three different materials (latex, nylon and optical fiber) and various diameters were used. In all experiments, deflections of the rods under their own weight are large compared to the radius of the cylindrical chamber R, that is $R \ll (B/\rho g R_0)^{1/4}$, where $B \sim E R_0^4$ is the bending rigidity of a rod with elastic modulus E, density ρ and cross-section radius $R_0 \ll R$. This condition ensures that gravity can be neglected. Rods also present variable intrinsic radii of curvature that depend on their stocking conditions before experiments. The intrinsic curvature R_i is determined by the natural curvature adopted by a rod deposited on a vibrating horizontal plane. Only the intrinsic radius of curvature of the optical fiber is independent of stocking conditions and can be considered as infinite. In the following, we are interested in packing properties for which the main control parameters are the aspect ratio H/R, the dimensionless intrinsic radius of curvature R_i/R and the friction of the rod on the container. The aspect ratio of the chamber is varied by using different plexiglass tubes of radius R varying from 13 mm to 100 mm and height H between the injection point and the bottom of the cavity varying from 10 mm to 130 mm.

A qualitative analysis of experimental results allows to distinguish two main regimes in the rod packing: an ordered phase, which consists of the formation of a regular coil against the walls of the cylindrical chamber and a disordered phase in which the packing of the rod occupies the space in an apparent random way (see fig. 1(c)). In the following, we aim at identifying and characterizing these two types of compaction as functions of the experimental parameters.

Ordered packing. – In this phase, a progressive coiling of the rod against the interior wall of the chamber takes place (see fig. 1(c)). Starting from the bottom of the cavity at an initial distance H from the injection point, spooling continues until a critical distance h_c is achieved for which the rod jumps inside the existing spool. At this critical point, two scenarios are observed: either the rod makes a new coil or starts to pack in a disordered way. Independently of the evolution of packing after the destabilisation has occurred, the critical height h_c was experimentally determined for various chamber sizes and intrinsic radii of curvature for the rods. To isolate the effect of each parameter, the compaction of elastic rods without intrinsic radius of curvature (that is with $R_i \to \infty$) was studied as a function of the sizes of the container. In this case, the scaled critical height h_c/R is found to increase with the initial distance H, having a minimal value $h_c/R \approx 1$ when $H \to h_c$. Actually, a large initial height H requires large number of windings in the coil before the critical h_c is achieved. The feeding system of fig. 1(a) induces torsion of the rod during injection. Assuming that each new winding twists the free of the rod by a fixed angle, the accumulated twist τ is then proportional to the total number of turns $n = (H - h)/(2R_0)$. Figure 2 shows the experimental results of h_c as a function of n_c.

Experiments on the variation of the critical height h_c with the intrinsic radius of curvature R_i show that h_c is approximately constant as long as $R_i \gg R$. However, h_c drastically increases when $R_i/R \lesssim 4$, reaching a maximum value $h_c/R \simeq 3$ for $R_i/R \simeq 3$. Further reduction of the intrinsic radius of curvature with respect to the radius of

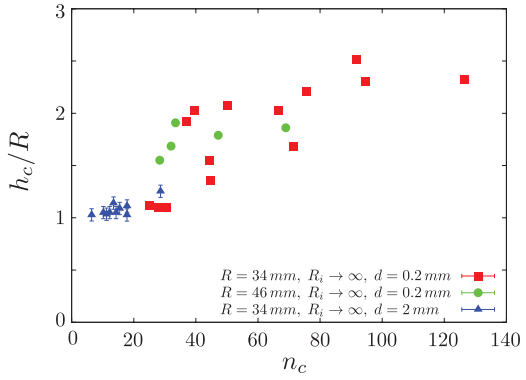

Fig. 2: (Colour on-line) Critical height h_c as a function of the critical winding number $n_c = (H - h_c)/(2R_0)$ for various rods made of materials without intrinsic curvature (that is with $R_i \to \infty$).

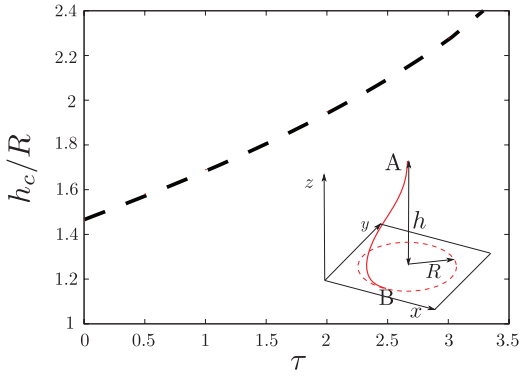

Fig. 3: (Colour on-line) The scaled critical height h_c/R as a function of the applied twist τ. The results are deduced from the numerical resolution of the elastic problem of a rod clamped at the injection point A and supported by the container at the top of the coil B (see the inset).

the cylindrical chamber leads to a disordered regime where no coiling states are observed.

The critical height h_c for the limit case $R_i \to \infty$ can be estimated by solving the elastic problem for the free part of the rod between the injection point and the first contact point with the container at the top of the coil (the curve AB in fig. 3). The dimensionless equilibrium equations of an element of a rod of arc length ds are given by [18–20]

$$\frac{\mathrm{d}\mathbf{r}}{\mathrm{d}s} \times \frac{\mathrm{d}^3\mathbf{r}}{\mathrm{d}s^3} + \tau \frac{\mathrm{d}^2\mathbf{r}}{\mathrm{d}s^2} = \mathbf{F} \times \frac{\mathrm{d}\mathbf{r}}{\mathrm{d}s}, \tag{1}$$

where $\mathbf{r}(s) = (x(s), y(s), z(s))$ is the position vector, τ is the twist and $\mathbf{F} = (F_x, F_y, F_z)$ is a constant force applied on the rod. Spatial quantities are dimensioned by the radius of the cylinder R and the force by B/R^2. The tangent vector of an inextensible rod can be characterized by two angles $\theta(s)$ and $\psi(s)$ through

$$x'(s) = \cos\theta\cos\psi, \quad y'(s) = \sin\theta\cos\psi, \quad z'(s) = \sin\psi, \tag{2}$$

where primes denote derivatives with respect to s. Using conditions (2), the projection of eq. (1) on the xy-plane and on the z-axis yields

$$\psi'' + \theta'^2 \sin\psi\cos\psi - \tau\theta'\cos\psi = (F_x\cos\theta + F_y\sin\theta)\sin\psi - F_z\cos\psi, \tag{3}$$

$$\theta''\cos\psi - 2\theta'\psi'\sin\psi + \tau\psi' = F_x\sin\theta - F_y\cos\theta. \tag{4}$$

To complete the formulation of the problem, one needs to specify the boundary conditions. The rod has a vertical tangent at the injection point A ($s = \ell$) and a horizontal tangent at the contact point with the cylinder B ($s = 0$):

$$\psi(0) = 0, \quad \psi(\ell) = \pi/2, \quad \theta(0) = \pi/2. \tag{5}$$

In addition, the length ℓ is a free parameter and the rod is supported at both endpoints. Therefore, the curvature $\psi'(\ell)$ at A is imposed by the injection nozzle and the principal curvature $\theta'(0)$ at B is imposed by the cylinder [20]:

$$\psi'(\ell) = 0, \quad \theta'(0) = -1. \tag{6}$$

Finally, the coordinates of the injection point A and of the contact point with the cylinder B are defined by $(1, 0, h_c)$ and $(0, 0, 0)$, respectively. This gives three additional constraints:

$$\int_0^\ell x'(s)\mathrm{d}s = 1, \quad \int_0^\ell y'(s)\mathrm{d}s = 0, \quad \int_0^\ell z'(s)\mathrm{d}s = h. \tag{7}$$

The equilibrium equations (3), (4) together with the boundary conditions (5)–(7) can be solved numerically for fixed values of τ and h. The length ℓ and the components of the force are an outcome of the resolution process.

Spooling is possible as long as the rod remains above the existing coil (*i.e.* the plane $z = 0$), which thus imposes a condition on the curvature at the contact point B. The mechanical stability of spooling is related to the sign of $\psi'(0)$ that defines the curvature of the rod along the z-axis at the contact point with the container: $\psi'(0) > 0$ (respectively, $\psi'(0) < 0$) corresponds to stable (respectively, unstable) configurations. Numerical results show that, for a fixed twist τ, the curvature $\psi'(0)$ is an increasing function of h and changes sign for a critical $h = h_c(\tau)$ which defines the threshold height above which ordered coiling configuration occurs.

Figure 3 shows that the stability threshold of a twist-free rod ($\tau = 0$) is obtained for a value of $h_c = 1.467R$, retrieving the result of coiling of a flexible rope on a surface when inertial and gravity effects are negligible [19]. This value is larger than the experimental one $h_c \simeq R$ (see fig. 2) indicating that the mechanical stability of spooling is closely influenced by friction of the rod with both the container and the previously formed coil. Nevertheless, fig. 3 shows that the critical height h_c/R increases with increasing applied twist τ which is qualitatively consistent with experimental observations of fig. 2, confirming the hypothesis of twist being the source of variation of the critical height h_c.

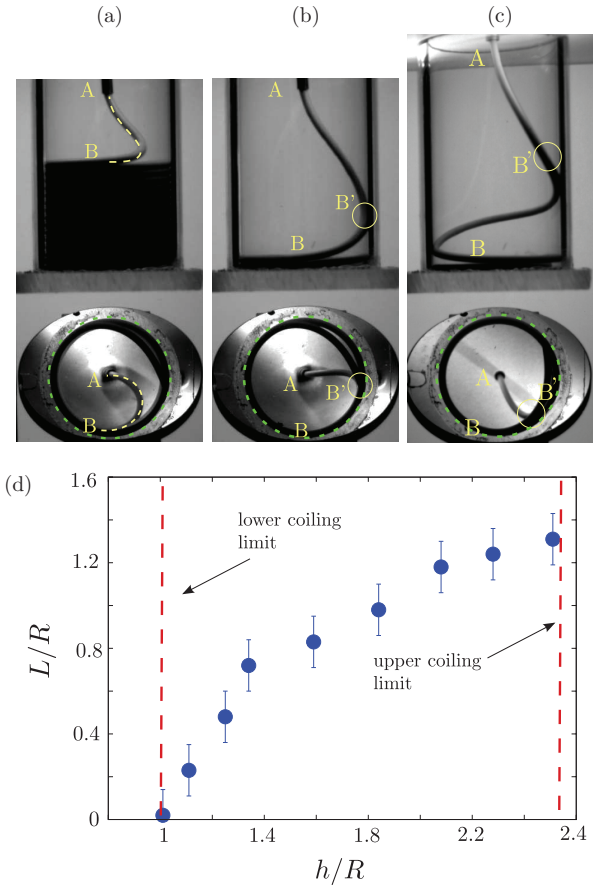

Fig. 4: (Colour on-line) (a)–(c) Lateral and bottom views of the rod during packing for various heights h. (a) $h \approx h_c$: the simultaneous inspection of both views shows that the contact with the container occurs at the point B that defines the end of the spool. (b) $h > h_c$: the rod contacts first the container at a point B′ defining a separate segment B′B in contact with the internal wall of chamber. (c) Above a critical height H_c: pressure on B′B is so large (and so is friction) that coiling is not possible. (d) Length L of the segment B′B as a function of the distance h between the injector and the coil. Lower (h_c) and upper limits (H_c) for ordered coiling to occur are shown.

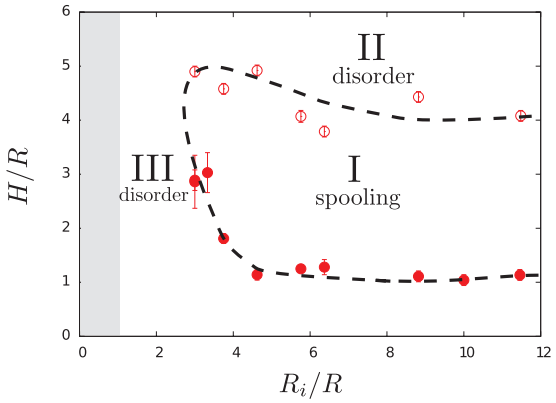

Fig. 5: (Colour on-line) Phase diagram of the different packing regimes as a function of the physical parameters H/R and R_i/R. The filled dots in the lower limit of the ordered coiling region correspond to the experimental critical values h_c for low twisted rods (small number of windings in the coil before h_c is reached). The empty dots in the upper limit correspond to the critical values H_c for the nylon-plexiglass configuration. The dashed line is a guide to the eye. The shadowed region corresponds to $R_i < R$ for which the rod can coil without even touching the walls of the container.

Experimental results show that for a coiled state to exist, the initial distance H should be larger than h_c, defining a necessary condition. However, there is also an upper limit for H beyond which the coiled state is not observed. Figures 4(a)–(c) show the initial stages of coiling for various distances h. For $h > h_c$, simultaneous lateral and bottom views of the system show that starting from the injection point A, the first contact of the rod with the inner wall of the container occurs at a point B′, where $\psi(\mathrm{B}') > 0$, that is different from the endpoint B of the existing coil, where $\psi(\mathrm{B}) = 0$. To achieve a coiled state the segment B′B of the rod should slide on the walls of the chamber overcoming friction forces induced by the normal forces of the container wall on the rod. Therefore, the coiled state depends on the material's friction coefficient and on the length L of the segment B′B that quantifies the magnitude of the applied pressure. Figure 4(d) shows the variation of L as a function of the distance h between the points A and B: it increases with h from 0 for $h \approx h_c$. When h reaches a critical value H_c, friction becomes so large that the segment B′B does not slide, forming first a helix standing against the chamber walls (see fig. 4(c)) and thus leading to a disordered packing of the rod.

Figure 5 summarizes the resulting phase diagram where the region of existence of coiled state is delimited by both h_c and H_c.

Disordered packing. – A disordered phase is considered to be any packing state that is different from regular coiling. It can occur after regular coiling or at the beginning of the compaction process. To illustrate better the dependence of ordered and disordered states on the experimental parameters, we shall make reference to the phase diagram shown in fig. 5. The lower limit of the ordered packing phase is determined by the critical height h_c for $\tau \to 0$ while the upper limit is fixed by H_c. It must be pointed out that the upper limit strongly depends on the sliding conditions of the rod over the interior walls (the upper limit of the phase diagram in fig. 5 corresponds to nylon on plexiglass friction conditions only).

To study the dynamical and possible statistical properties of both ordered and disordered configurations, we focus on the analysis of the dynamics of the rod at the entrance of the chamber. We track the position of the intersection of the rod with a horizontal plane a few millimeters under the injector (the dotted line (A) in fig. 1(b)). We will particularly focus on the temporal evolution of two parameters: the distance $r(t)$ of the rod to the axis of the chamber and the coiling direction $\Omega(t)$ defined by

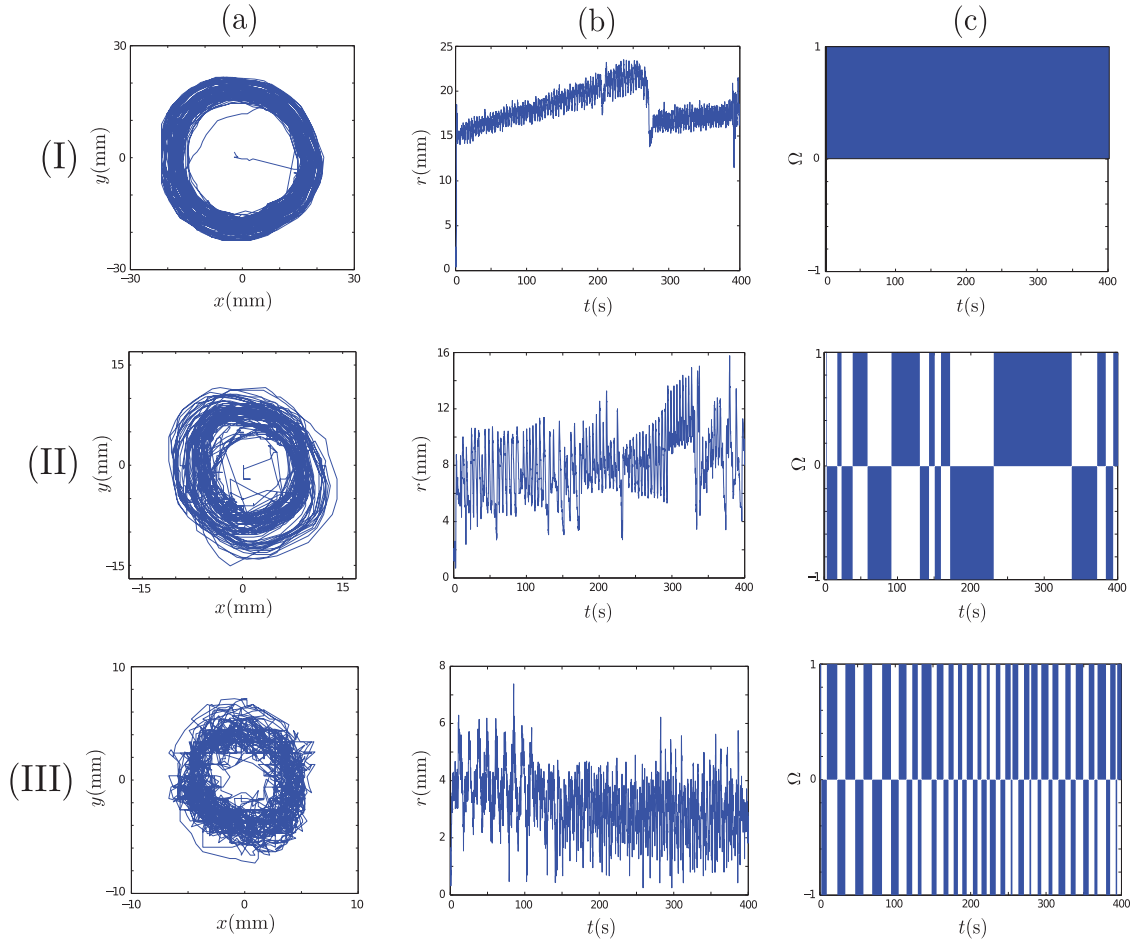

Fig. 6: (Colour on-line) Three experimental realisations of packing generated in the different regions defined in fig. 5. From top to bottom: ordered coiling (region I), and disordered packing in regions II and III, respectively. From left to right, (a) trajectory of the rod at the entrance of the cavity and the corresponding dynamic evolutions of $r(t)$ (b) and $\Omega(t)$ (c).

$\Omega(t) = +1$ (respectively, $\Omega(t) = -1$) for counterclockwise (respectively, clockwise) rotation. Each region I, II and III as defined in fig. 5 can be identified by the corresponding temporal behavior of r and Ω.

Figure 6(I) shows a typical signal of the ordered coiling state (region I) and the evolution of the corresponding $r(t)$ and $\Omega(t)$. The ordered phase is characterized by a radius $r(t)$ that increases gradually with time as a result of the coiling process: the more the top of the coil approaches the injection point, the wider the turns of the rod at the entrance are. The evolution of $r(t)$ presents also "jumps" when the critical height h_c is reached and then a new coil eventually starts inside the previous one (*e.g.*, event at $t \simeq 260\,\mathrm{s}$ in fig. 6(Ib)). Moreover, this spooling phase in characterised by Ω that does not change sign meaning that the rod always rotates in the same direction. Figure 6 also shows that different evolutions of the system are observed in the disordered regions II and III. In both cases the evolution of $r(t)$ is quite random and does not exhibit definite measurable characteristics. However, there are important differences in the evolution of $\Omega(t)$. While Ω changes randomly in region II, a well-defined periodicity in the changes of rotation direction emerges in region III. Despite the apparent disordered packing in the container, some order is revealed in the filling dynamics.

Figure 7 shows the probability density functions (pdfs) of the rotating duration period Δt in either clockwise or counter-clockwise directions for a rod packed in region III. Noticing that in this region, the intrinsic radius of curvature of the rod R_i is of the same order as the radius of the cylindrical cavity R, the duration period is dimensioned by R_i/v where v is the injection speed. Figure 7 shows that the pdfs for various R_i/R and H/R exhibit a peak around 2π. This result is particularly important because it reveals the formation of perversions on the rod distant by approximately $2\pi R_i$. Perversions are local structures that connect two helices of different chirality. Intrinsically curved rods tend to get rid of excess torsion by forming perversions at points where the twisting moments are negligible [20,21]. This phenomenon shows up in twisting tendrils of climbing plants and in kinky telephone cords. Analytical solutions for a twisted intrinsically curved rod shows that the length between perversions is slightly larger to $2\pi R_i$ [20,21], which is similar to our

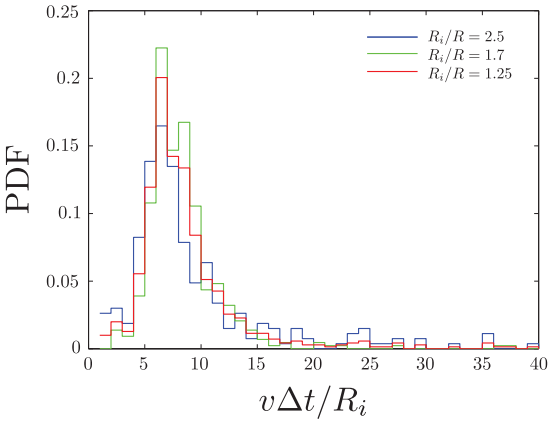

Fig. 7: (Colour on-line) Probability density functions (pdfs) of the scaled rotating duration period $v\Delta t/R_i$ extracted from the dynamics of $\Omega(t)$ for a rod packed in region III. Each data set corresponds to a given value of R_i/R for which the value of H is varied from 5 mm to 13 mm with increments of 1 mm.

result for disordered compaction in region III. In this region, perversion is thus the driving mechanism leading to a disordered phase that is characterized by spooling with periodic alternating chirality.

Conclusion. – We have characterized experimentally the packing of an elastic rod in a rigid cylinder as a function of the aspect ratio of the container and the intrinsic curvature of the rod. We show that the packing process depends only on the geometrical properties of the system and on friction between the rod and the cylinder, independent of the rigidity of the rod. We have determined a phase diagram (fig. 5) in which each frontier defines the transition from spooling to disordered packing scenarios. For cavities with small aspect ratios, experiments and numerical simulations have shown that the coiling state is dictated by the mechanical stability of the free rod between the injector and the last turn of the coil (frontier defined by the filled dots in fig. 5). For long containers, the friction of the rod against the wall prevents stacking of the rod and leads to a disordered packing (frontier between I and II). The study of the injection dynamics revealed another scenario of transition to disordered configurations (frontier between I and III). In the region of the phase diagram where the radius of the cylinder compares to the intrinsic radius of the rod, the rods form perversions while injected in the confined space. We were able to differentiate between these two disordered regimes by analyzing the dynamics of the rod at the injection point. While the disordered regime (II) does not reveal any measurable characteristics, a temporal order emerges from the packing dynamics in the disordered regime (III) that is cadenced by the formation of the perversions.

REFERENCES

[1] Kobayashi H., Kresling B. and Vincent J. F. V., *Proc. R. Soc. London, Ser. B*, **265** (1998) 147.
[2] Couturier E., du Pont S. C. and Douady S., *PLoS ONE*, **4** (2009) e7968.
[3] Miura K., *Proceedings of the 31st Congress of the International Astronautical Federation*, Vol. **IAF-80-A 31** (American Institute for Aeronautics and Astronautics, New York) 1980.
[4] Thompson J. M. T., Silveira M., van der Heijden G. H. M. and Wiercigroch M., *Proc. R. Soc. London, Ser. A*, **468** (2012) 1591.
[5] Purohit P. K., Inamdar M. M., Grayson P. D., Squires T. M., Kondev J. and Phillips R., *Biophys. J.*, **88** (2005) 851.
[6] Kindt J., Tzlil S., Ben-Shaul A. and Gelbart W. M., *Proc. Natl. Acad. Sci. U.S.A.*, **98** (2001) 13671.
[7] Katzav E., Adda-Bedia M. and Boudaoud A., *Proc. Natl. Acad. Sci. U.S.A.*, **103** (2006) 18900.
[8] Matan K., Williams R. B., Witten T. A. and Nagel S. R., *Phys. Rev. Lett.*, **88** (2002) 076101.
[9] Thiria B. and Adda-Bedia M., *Phys. Rev. Lett.*, **107** (2011) 025506.
[10] Blair D. L. and Kudrolli A., *Phys. Rev. Lett.*, **94** (2005) 166107.
[11] Andresen C. A., Hansen A. and Schmittbuhl J., *Phys. Rev. E*, **76** (2007) 026108.
[12] Deboeuf S., Adda-Bedia M. and Boudaoud A., *EPL*, **85** (2009) 24002.
[13] Adda-Bedia M., Boudaoud A., Boué L. and Deboeuf S., *J. Stat. Mech.* (2010) P11027.
[14] Deboeuf S., Katzav E., Boudaoud A., Bonn D. and Adda-Bedia M., *Phys. Rev. Lett.*, **110** (2013) 104301.
[15] Bayart E., Deboeuf S., Corson F., Boudaoud A. and Adda-Bedia M., *EPL*, **95** (2011) 34002.
[16] Donato C. C., Gomes M. A. F. and de Souza R. E., *Phys. Rev. E*, **67** (2003) 026110.
[17] Stoop N., Najafi J., Wittel F. K., Habibi M. and Herrmann H. J., *Phys. Rev. Lett.*, **106** (2011) 214102.
[18] Landau L. D. and Lifshitz E. M., *Theory of Elasticity* (Butterworth-Heinemann, Oxford) 1986.
[19] Mahadevan L. and Keller J. B., *Proc. R. Soc. London, Ser. A*, **452** (1996) 1679.
[20] Audoly B. and Pomeau Y., *Elasticity and Geometry* (Oxford University Press, Oxford) 2011.
[21] McMillen T. and Goriely A., *J. Nonlinear Sci.*, **12** (2002) 241.